applied sciences

MDPI

Article

Low-Carbon Economic Dispatch of Integrated Energy Systems in Industrial Parks Considering Comprehensive Demand Response and Multi-Hydrogen Supply

Bohua Su [1], Ruiqi Wang [2], Ming Wang [1,*], Mingyuan Wang [1], Qianchuan Zhao [3], Yisheng Lv [4] and He Gao [5]

[1] School of Information and Electrical Engineering, Shandong Jianzhu University, Jinan 250101, China
[2] State Grid Shandong Integrated Energy Services Co., Ltd., Jinan 250001, China
[3] Department of Automation, Tsinghua University, Beijing 100084, China
[4] Institute of Automation, Chinese Academy of Sciences, Beijing 100190, China
[5] Shandong Zhengchen Technology Co., Ltd., Jinan 250101, China
* Correspondence: xclwm@sdjzu.edu.cn

Abstract: To address the increasing hydrogen demand and carbon emissions of industrial parks, this paper proposes an integrated energy system dispatch strategy considering multi-hydrogen supply and comprehensive demand response. This model adopts power-to-gas technology to produce green hydrogen, replacing a portion of gray hydrogen and incorporates a carbon capture system to effectively reduce the overall carbon emissions of the industrial park. Meanwhile, incentive-based and price-based demand response strategies are implemented to optimize the load curve. A scheduling model is established targeting the minimization of procurement, operation, carbon emission, and wind curtailment costs. The case study of a northern industrial park in China demonstrates that the joint supply of green and gray hydrogen reduces carbon emissions by 40.98% and costs by 17.93% compared to solely using gray hydrogen. The proposed approach successfully coordinates the economic and environmental performance of the integrated energy system. This study provides an effective scheduling strategy for industrial parks to accommodate high shares of renewables while meeting hydrogen needs and carbon reduction targets.

Keywords: integrated energy systems; demand response; tiered carbon trading; green hydrogen substitution

Citation: Su, B.; Wang, R.; Wang, M.; Wang, M.; Zhao, Q.; Lv, Y.; Gao, H. Low-Carbon Economic Dispatch of Integrated Energy Systems in Industrial Parks Considering Comprehensive Demand Response and Multi-Hydrogen Supply. *Appl. Sci.* **2024**, *14*, 2381. https://doi.org/10.3390/app14062381

Academic Editors: Gheorghe Grigoras and Cristian-Dragoș Dumitru

Received: 28 January 2024
Revised: 2 March 2024
Accepted: 7 March 2024
Published: 12 March 2024

1. Introduction

Given the increasing severity of climate change and environmental degradation, carbon emissions have emerged as a prominent issue that has garnered global attention. China has established targets to reach carbon peaking by 2030 and carbon neutrality by 2060 [1]. This commitment is driving the global adoption of renewable energy and promoting an active transition toward sustainable energy sources. In light of this context, the integrated energy system (IES) has gained significant recognition for its potential to establish energy complementarity and improve energy usage [2,3]. Moreover, coastal regions reap the advantages of ample sustainable resources like wind and solar energy, while certain chemical industrial zones exhibit a need for hydrogen. As a result, the technology for generating power from renewable energy sources and producing hydrogen is becoming increasingly important. However, some industrial areas excessively depend on gray hydrogen, which is known for its low cost but significant levels of carbon emissions. To address the "dual-carbon" objectives, it is crucial to examine the carbon mitigation advantages of utilizing renewable energy for the production of green hydrogen, with the aim of attaining both economic viability and minimal carbon emissions.

Hydrogen, as a clean energy source with high energy density and zero carbon emissions, has long been a focal point of research. Lepage et al. employed thermochemical,

biological, and electrochemical methods for hydrogen production from biomass, demonstrating the superior effectiveness of thermochemical approaches in biomass hydrogenation [4]. Li et al. conducted a comparative study on the carbon emissions of hydrogen production from biomass and coal, affirming a 75.4% reduction in carbon emissions for biomass hydrogenation compared to coal hydrogenation [5]. Alabbadi et al. investigated nuclear-powered hydrogen production, considering the utilization of the advanced pressurized water reactor (APWR) and high-temperature gas-cooled reactor (HTGR) to provide energy for electrolysis [6]. El-Emam et al. discussed the cost estimation and safety aspects of large-scale nuclear hydrogen production using various nuclear propulsion technologies, presenting the current research status of thermochemical cycles for hydrogen production [7]. However, in contrast, biomass hydrogen production yields are relatively low and insufficient to meet the hydrogen demand of the industrial park. While nuclear-powered hydrogen production allows for large-scale hydrogen generation, it involves safety risks and waste management challenges and is not applicable to all scenarios. In comparison to these alternatives, wind-powered hydrogen production, despite its drawbacks such as susceptibility to weather fluctuations and the need for upfront infrastructure investments, offers advantages in terms of widely distributed wind energy resources and high flexibility. Moreover, the hydrogen output is sufficient to meet a portion of the industrial park's hydrogen demand. Therefore, this study opts for the investigation of wind-powered hydrogen production, which is adaptable to a wide range of scenarios and exhibits high hydrogen production capacity. Wind power, in this context, requires the use of power-to-gas (P2G) technology for hydrogen extraction.

Prior research has investigated the P2G technology. Liu tackled the issue of bidirectional energy flow between the electricity and natural gas systems using a multi-objective black hole particle swarm optimization approach [8]. Additionally, the study suggested a gas demand management strategy to ensure a balanced gas flow. Yang et al. used a blend of P2G technology and gas-fired power plants to create a framework that measures its ability to reduce carbon emissions and utilize renewable energy [9]. To quantify the flexibility of P2G units in the electricity–gas–hydrogen-integrated distribution system, Antonella established a multi-energy vector framework containing multiple P2G units and assessed it through a node operating envelope (NOE) [10]. Son et al. introduced the potential renewable penetration index (PRPI) to select the appropriate capacity for P2G facilities, aiming to enhance the penetration of renewable energy sources [11]. Nevertheless, with the increase in power consumption, the electrolysis efficiency of water gradually decreases from around 85% to 65%, leading to a gradual decline in the overall efficiency of P2G systems [12,13]. Thus, Zhang et al. enhanced the process of P2G by dividing it into two stages: electrolytic hydrogen production and hydrogen methanation. This approach established a low-carbon economic scheduling model for regional integrated energy systems, taking into account heating networks and P2G [14]. To efficiently utilize the hydrogen produced through water electrolysis in P2G devices, Mansouri injected the generated hydrogen into a gas-fired device, thereby enhancing the efficiency of the gas-fired apparatus [15]. The hydrogenation process can utilize a carbon capture system (CCS) to obtain the necessary carbon source [16]. Alizad et al. employed a stochastic dynamic programming approach to design a P2G integrated energy hub system, aiming to investigate the impact of P2G-CCS systems on carbon reduction and system operational costs [17]. Reference [18] considered the coupling of CCS and P2G, establishing a bi-level optimization scheduling model, and verified that the coupling of P2G-CCS can enhance the economic viability and the ability to accommodate wind and solar power in the comprehensive energy system. However, the aforementioned studies primarily focus on the impact of P2G on improving the economic efficiency of the system, neglecting the influence of utilizing hydrogen produced through P2G as a hydrogen source to reduce carbon emissions in industrial production.

Demand response technology is an essential method used in the IES to flatten load curves and optimize the economic functioning of the system [19]. Demand response seeks to achieve peak shaving and valley filling by directing user behavior and facilitating

coordinated interaction between supply and demand. A customer satisfaction model is introduced in [20], which enhances the existing load models for demand response in electricity, gas, cooling, and heating. This model also takes into account price-based demand response. To investigate the economic and environmental potential of price-responsive demand response, Fleschutz et al. proposed two preference-based methods to approximate the hourly marginal emission factor (MEF) and demonstrated that when carbon prices are sufficient, price-responsive demand response can be an effective tool for improving both economic and environmental outcomes [21]. Pandey et al. employed the microeconomic behavioral framework of overlapping generations (OLG) to establish a price-responsive demand model, accurately representing customer load behavior [22]. The objective of [23] is to decrease system running expenses and manage the surplus electricity generated by wind power by integrating price-based demand response with a hydrogen energy storage system. Tavakkoli et al. introduced incentive-based demand response and employed the Stackelberg game method to encourage residential users to actively participate in demand response programs [24]. Tilburg et al. proposed a decentralized multi-agent reinforcement learning method for incentive-based demand response, aiming to reduce energy consumption and prevent grid congestion [25]. To encourage more users to participate in demand response, Raman et al. employed real-time feedback to adaptively modify participants' incentive measures and enhance the flexibility of the distribution system's demand through the integration of electric vehicles [26]. However, the existing literature primarily concentrates on examining the influence of demand response on the demand side while overlooking the evaluation of energy-saving potential among various types of demand response.

Therefore, this study aims to realize the comprehensive utilization of P2G technology, demand response, and carbon capture and storage means, optimize the operation of the energy system in the industrial park, and achieve the win-win research goals of saving energy, reducing carbon emissions, and gaining economic benefits. To do so, this study utilizes the aforementioned research and develops a thorough energy system model for an industrial park that integrates P2G and CCS. The model considers the carbon reduction advantages of substituting green hydrogen, linking power-to-gas with carbon capture and storage, implementing a hierarchical carbon trading system, and the influence of complete demand response on the economic and environmental performance of the system. A scheduling model for optimization is formulated, aiming to minimize the total cost of procurement, operation and maintenance, carbon emissions, and wind abandonment. The case study incorporates many control groups to validate the superiority of the proposed low-carbon scheduling technique. This paper's primary contributions are as follows:

(i) Suggesting a production technique that makes use of several hydrogen sources. This study explores the substitution of green hydrogen for a portion of traditional gray hydrogen as the hydrogen source, combined with a comprehensive assessment of the carbon reduction benefits of green hydrogen using a stepwise carbon trading approach. Furthermore, the study conducted an in-depth investigation into the effects of substituting green hydrogen for a portion of gray hydrogen on "demand response" and the coupling of P2G and CCUS.

(ii) The research examines the effects of incentive-based demand response and price-based demand response on the economic performance of the system. It investigates the energy-saving potential of various types of demand response. This study measures the impact of incentive strategies and price systems on the energy consumption of the industrial park.

(iii) Implementation of a highly efficient CCS technique to capture and recycle CO_2, hence improving the economic viability of the system. The integration of P2G technology with CCS allows for the creation of a closed-loop system that effectively reduces carbon emissions in the industrial park. This integration also enhances the economic efficiency of the overall system.

The remaining sections of this paper are organized as follows: Section 2 introduces the full energy system model incorporating hydrogen, which encompasses the modeling

of key equipment; Section 3 provides frameworks for price-based and incentive-based demand response; Section 4 explores the optimization goals and limitations, establishing the framework for the optimization scheduling model; Section 5 performs simulated verification of the proposed optimization scheduling approach to showcase its efficacy; Section 6 examines the merits, drawbacks, and advancements of the suggested approaches; and Section 7 provides a concise overview of the research conducted in this research.

2. Comprehensive Hydrogen-Integrated Energy System Model

A detailed depiction of the hydrogen-integrated energy system designed is provided in this paper, as seen in Figure 1. The supply side of the system consists of the power grid, wind turbine units, gas network, and industrial gray hydrogen. The load side comprises electric, gas, cooling, heating, and hydrogen loads. The power grid, gas turbine (GT), wind turbine (WT), and energy storage (ES) equipment provide the electric load. The gas load is supplied by the gas network and methane reactor (MR). The heat load is sustained by waste heat boilers (HRSG), gas boilers (GB), and thermal storage (HS) apparatus. The cooling need is met by absorption chillers (AC), electric chillers (EC), and cold storage (CS) equipment. The hydrogen demand is fulfilled by industrial gray hydrogen, electrolyzers (EL), and hydrogen storage (QS) apparatus. GT, AC, and HRSG collectively constitute a combined cooling, heating, and power (CCHP) unit.

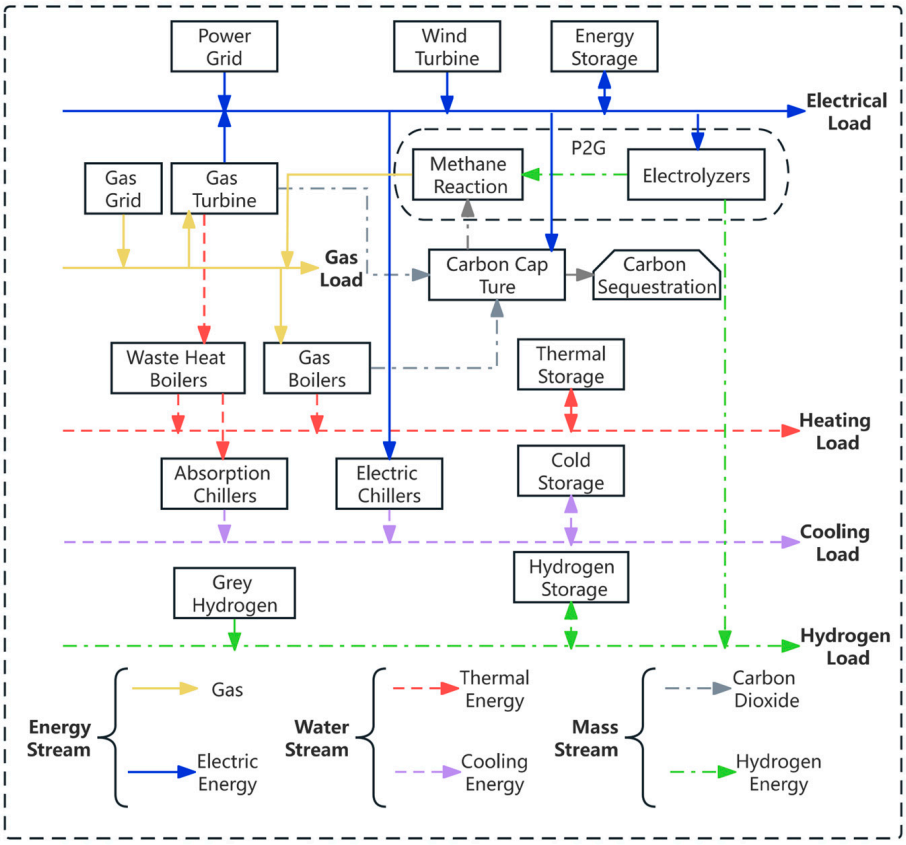

Figure 1. Architecture of an integrated energy system.

2.1. P2G-CCS Coupling Model

2.1.1. CCS Model

CCS essentially comprises two distinct stages: carbon capture and carbon sequestration.

During the carbon capture phase, carbon dioxide emitted by industries is caught and separated into two distinct streams. A single stream is conveyed to the P2G equipment, more specifically the methane reactor, where it undergoes a reaction with hydrogen to generate methane, so enabling the cyclic usage of CO_2. The energy usage during this stage

is categorized into operational and fixed components. Operational energy consumption is calculated by measuring the quantity of carbon dioxide emitted, whereas fixed energy consumption results from alterations in the regular functioning of equipment, leading to extra expenses. The precise formulation is as follows:

$$\begin{cases} P_{\mathrm{CCS}}(t) = P_{\mathrm{run}}(t) + P_{\mathrm{CCS}}^{b} \\ P_{\mathrm{run}}(t) = e_{\mathrm{ccs}} M_{\mathrm{CCS}}(t) \\ M_{\mathrm{CCS}}(t) = \eta_{\mathrm{ccs}} e_{\mathrm{g2c}} G_{\mathrm{g}}(t) \end{cases} \tag{1}$$

where $P_{\mathrm{CCS}}(t)$ represents the total energy consumption of the carbon capture system at time t, $P_{\mathrm{run}}(t)$ denotes the operational energy consumption at time t, P_{CCS}^{b} signifies the fixed energy consumption of the carbon capture system, typically a constant; e_{CCS} indicates the electricity consumption per unit mass of CO_2 captured, $M_{\mathrm{CCS}}(t)$ represents the mass of CO_2 captured by the carbon capture system at time t; η_{ccs} denotes the efficiency of the carbon capture system; e_{g2c} represents the mass of CO_2 generated per unit volume of natural gas combustion; and $G_{\mathrm{g}}(t)$ represents the natural gas consumption at time t by the gas-consuming equipment. This equation signifies that the input for the carbon capture component is the quantity of carbon dioxide emitted through the combustion of natural gas by the system. While its operation results in an increase in a portion of the system's operational costs, it significantly reduces the overall carbon emissions of the system.

The remaining portion of the captured carbon dioxide Is subjected to sequestration using a carbon dioxide compressor. The CO_2 is pressurized to achieve a high-density state and subsequently sent underground to avert its emission into the atmosphere. The formula representing this procedure is as follows:

$$\begin{aligned} M_{\mathrm{CCS}}(t) &= m_{\mathrm{MR}}(t) + m_{\mathrm{f}}(t) \\ C_{\mathrm{f}}^{CO_2} &= c_{\mathrm{f}} \sum_{\mathrm{t}=1}^{T} m_{\mathrm{f}}(t) \end{aligned} \tag{2}$$

where $m_{\mathrm{MR}}(t)$ and $m_{\mathrm{f}}(t)$ represent the input of methane into the reactor, the mass of CO_2 captured and sequestered at time t, respectively; $C_{\mathrm{f}}^{CO_2}$ denotes the cost of carbon sequestration, and c_{f} signifies the cost of sequestering one unit of CO_2 mass.

2.1.2. P2G Model

The P2G system uses electrical energy to convert collected CO_2 from CCS into natural gas. The produced natural gas is subsequently reintroduced into gas-consuming equipment, enabling the cyclical usage of carbon. In order to fully evaluate the environmental advantages of green hydrogen, the P2G process is subdivided into two distinct stages: electrolytic hydrogen production and methane generation. The equation representing the conversion model for electrolytic hydrogen production is as follows:

$$Q_{\mathrm{P2H}}(t) = \eta_{\mathrm{P2H}} P_{\mathrm{P2H}}(t) \tag{3}$$

where $Q_{\mathrm{P2H}}(t)$ represents the mass of hydrogen produced by the P2G device during the time interval t; η_{P2H} denotes the conversion efficiency of electrolysis to hydrogen at time t; and $P_{\mathrm{P2H}}(t)$ signifies the power consumption of the P2G device at time t.

The hydrogen methanation process achieves coupling between P2G and CCS by absorbing the CO_2 captured from GB and GT. Simultaneously, it generates natural gas, supplying gas to GB and GT, thereby cyclically utilizing CO_2 and reducing the overall carbon emissions of the system. The expression for the methane generation process is as follows:

$$\begin{aligned} Q_{\mathrm{H2G}}(t) &= Q_{\mathrm{P2H}}(t) - Q_n(t) \\ G_{\mathrm{MR}}(t) &= \eta_{\mathrm{MR}} Q_{\mathrm{H2G}}(t) \\ m_{\mathrm{MR}}(t) &= \frac{3600 Q_{\mathrm{H2G}}(t)}{l_{\mathrm{CH_4}}} \rho_{\mathrm{CO_2}} \end{aligned} \tag{4}$$

where $Q_{H2G}(t)$ and $Q_n(t)$ represent the hydrogen consumption through methanation and the mass supplied to the user during time interval t, respectively; η_{MR} denotes the conversion efficiency of methanation at time t; $G_{MR}(t)$ signifies the gas production from methanation at time t; l_{CH_4} represents the heating value of natural gas; and ρ_{CO_2} denotes the density of CO_2. This system of equations represents the process of P2G methane reforming, with the input parameter being the mass of hydrogen consumed in the methanation process. The final equation in this system indicates that the CO_2 feedstock for methanation is sourced from CCS, highlighting the coupling of P2G and CCS. The P2G process, through methanation, consumes a portion of CO_2, thereby reducing the cost associated with carbon sequestration and positively impacting the economic efficiency of the system.

Hydrogen Storage Tank Model:

$$\begin{cases} E_{H_2}^{\min} \le E_{H_2}(t) \le E_{H_2}^{\max} \\ E_{H_2}(t+1) = \eta_{H_2}^{c} P_{H_2}^{c}(t) + P_{H_2}^{d}(t)/\eta_{H_2}^{out} \\ \lambda_{H_2} P_{H_2}^{c,\min}(t) \le P_{H_2}^{c}(t) \le \lambda_{H_2} P_{H_2}^{c,\max}(t) \\ (1-\lambda_{H_2}) P_{H_2}^{d,\min}(t) \le P_{H_2}^{d}(t) \le (1-\lambda_{H_2}) P_{H_2}^{d,\max}(t) \end{cases} \tag{5}$$

where $E_{H_2}(t)$ represents the hydrogen storage capacity of the storage tank at time t; $E_{H_2}^{\min}$ and $E_{H_2}^{\max}$ denote the upper and lower limits of the hydrogen storage capacity, respectively; $\eta_{H_2}^{c}$ and $\eta_{H_2}^{d}$ represent the efficiency of hydrogen storage and release, respectively; $P_{H_2}^{c}(t)$ and $P_{H_2}^{d}(t)$ represent the hydrogen storage and release power of the storage tank at time t, respectively; $P_{H_2}^{c,\min}$, $P_{H_2}^{c,\max}$, $P_{H_2}^{d,\min}$ and $P_{H_2}^{d,\max}$ represent the maximum and minimum values of the storage and release power, respectively; to prevent simultaneous hydrogen storage and release, λ_{H_2}, a binary variable, is equal to 1 during hydrogen storage and 0 during hydrogen release.

2.2. Tiered Carbon Trading Model

The tiered carbon trading approach, similar to tiered electricity pricing, seeks to gradually motivate consumers to decrease carbon emissions by establishing varying levels of carbon costs. This approach utilizes a tiered carbon trading system that incorporates gratuitous quotas. If the system's carbon emissions fall below the assigned quota, any excess carbon allowances can be sold on the trading market to generate profit. If, on the other hand, the carbon emissions of the system surpass the assigned limit, the corresponding carbon allowances must be bought back. The formula for computing carbon allowances during a schedule cycle is as follows:

$$E_C = \sum_{t=1}^{T} \lambda_{c2e} P_{cchp}(t) + \lambda_{c2h} H_{cchp}(t) + \lambda_{GB} H_{gb}(t) + \lambda_e P_{buy}(t) + \lambda_q Q_{buy}(t) \tag{6}$$

where E_C represents the carbon quota within a scheduling cycle; λ_{c2e} and λ_{c2h} denote the allocated quotas for CCHP unit's unit electricity and thermal power, respectively; λ_{GB} represents the allocated quota for the gas boiler's unit thermal power; λ_e and λ_q represent the allocated quotas for purchased unit electricity and unit mass of gray hydrogen, respectively; $P_{cchp}(t)$ and $H_{cchp}(t)$ represent the electricity and heat power generated by the CCHP unit at time t; $H_{gb}(t)$ represents the heat power generated by the gas boiler during time interval t; $P_{buy}(t)$ and $Q_{buy}(t)$ denote the purchased electricity power and the mass of purchased gray hydrogen at time t, respectively.

Actual Carbon Emission:

$$M_{real}(t) = M_{total}(t) - M_{CCS}(t) \tag{7}$$

where $M_{real}(t)$ represents the actual carbon emissions of the system at time t, and $M_{total}(t)$ represents the total carbon emissions generated by the system at time t.

The tiered carbon trading cost expression is as follows:

$$C_{\mathrm{p}}^{CO_2}(t)=\begin{cases}\chi[M_{\mathrm{real}}(t)-E_{\mathrm{C}}] & M_{\mathrm{real}}(t)-E_{\mathrm{C}}\le l\\ \chi(1+\varphi)[M_{\mathrm{real}}(t)-E_{\mathrm{C}}-l]+\chi l & l\le M_{\mathrm{real}}(t)-E_{\mathrm{C}}\le l\\ \chi(1+2\varphi)[M_{\mathrm{real}}(t)-E_{\mathrm{C}}-2l]+\chi(2+\varphi)l & 2l\le M_{\mathrm{real}}(t)-E_{\mathrm{C}}\le 3l\\ \chi(1+3\varphi)[M_{\mathrm{real}}(t)-E_{\mathrm{C}}-3l]+\chi(3+3\varphi)l & 3l\le M_{\mathrm{real}}(t)-E_{\mathrm{C}}\le 4l\\ \chi(1+4\varphi)[M_{\mathrm{real}}(t)-E_{\mathrm{C}}-4l]+\chi(4+6\varphi)l & M_{\mathrm{real}}(t)-E_{\mathrm{C}}\ge 4l\end{cases} \quad (8)$$

where $C_{\mathrm{p}}^{CO_2}(t)$ represents the stepwise carbon trading cost at time t; χ represents the carbon trading base price; l represents the interval length; φ represents the rate of price increase after an increase in carbon emissions. This equation set represents the input values as the actual carbon emissions of the system. Based on the actual carbon emissions, it establishes five stages with incrementally increasing carbon emission prices. As the carbon emissions increase, the system costs also rise. Therefore, to enhance economic efficiency, the system automatically reduces carbon emissions, achieving a balance between economic viability and carbon emissions.

3. Demand Response Models

Demand response is an essential method of enhancing energy efficiency by modifying consumer behavior to align with changes in supply and demand. This study focuses on two types of demand response: incentive-based demand response and price-based demand response. The difference between these two types of demand response lies in the fact that incentive-based demand response encourages consumer participation in energy management through various incentives, such as discounts, subsidies, or other motivating measures. On the other hand, price-based demand response involves direct adjustments to electricity prices, altering user electricity consumption behavior through price fluctuations to achieve more economical electricity usage and energy conservation.

3.1. Incentive-Based Demand Response Model

Incentive-based demand response offers rewards or incentives to motivate energy consumers to actively decrease their electricity usage during peak hours or critical situations, hence improving system efficiency [27]. The incentive cost is a measure of how effective load reduction participation is in scheduling. The cost of compensation for incentive-based response is expressed as follows:

$$C_{\mathrm{cut}}=c_{\mathrm{cut}}\sum_{t=1}^{T}\Delta L_{\mathrm{e}}^{t} \quad (9)$$

where C_{cut} represents the compensation cost for user participation in incentive response; c_{cut} represents the incentive compensation cost per unit power; $\Delta L_{\mathrm{e}}^{t}$ represents the load reduction amount of user participation in incentive response during time interval t; T represents one scheduling cycle, which is equivalent to 24 h.

The adjusted electric load, considering the incentive-based demand response, is calculated as follows:

$$\begin{cases} L_{\mathrm{e}}^{t}=L_{\mathrm{e},0}^{t}-\Delta L_{\mathrm{e}}^{t}\\ 0\le\Delta L_{\mathrm{e}}^{t}\le\Delta L_{\mathrm{e}}^{t,\max}\end{cases} \quad (10)$$

where L_{e}^{t}, $L_{\mathrm{e},0}^{t}$ and $\Delta L_{\mathrm{e}}^{t,\max}$ represent the user electricity load after incentive demand response at time t, the electricity load before demand response at time t, and the upper limit of electricity load change, respectively.

3.2. Price-Based Demand Response Model

The price-based demand response model employs time-of-use pricing. In order to optimize the load curve, a portion of the power load is transferred to off-peak hours during times of high prices [28]. In the field of price elasticity theory, the demand price elasticity coefficient is a crucial parameter employed to quantify the responsiveness of electricity demand to variations in price. The demand price elasticity coefficient can be mathematically modeled using the following equation:

$$e^{ij} = \frac{\Delta P_e^i / P_e^{i,0}}{\Delta \lambda^j / \lambda^{j,0}} \tag{11}$$

where e^{ij} represents the demand price elasticity coefficient; $P_e^{i,0}$ and $\lambda^{j,0}$ represent the electricity load before participating in price-based demand response at time i and the electricity price at time j; ΔP_e^i and $\Delta\lambda^j$ respectively represent the change in electricity load after price-based demand response at time i, and the change in electricity price at time j.

In order to divide a schedule cycle into peak, off-peak, and valley phases, we utilize the demand price elasticity coefficient to create a matrix that depicts the correlation between user demand and energy prices. The formulation of the Price Elasticity Matrix is as follows:

$$E = \begin{bmatrix} e^{pp} & e^{pf} & e^{pv} \\ e^{fp} & e^{ff} & e^{fv} \\ e^{vp} & e^{vf} & e^{vv} \end{bmatrix} \tag{12}$$

where e^{pp}, e^{ff} and e^{vv} represent the self-response demand price elasticity coefficients during peak, flat, and trough hours, respectively; e^{pf}, e^{pv} and e^{fv} represent the price elasticity of demand for peak-flat, peak-trough, and flat-trough interactions, respectively. The meanings of other coefficients are similar.

Utilizing the Price Elasticity Matrix, we establish the demand response model for electric load:

$$\begin{bmatrix} P_e^p \\ P_e^f \\ P_e^v \end{bmatrix} = diag(P_e^{p,0}, P_e^{f,0}, P_e^{v,0}) E \begin{bmatrix} \frac{\Delta\lambda^p}{\lambda^{p,0}} \\ \frac{\Delta\lambda^f}{\lambda^{f,0}} \\ \frac{\Delta\lambda^v}{\lambda^{v,0}} \end{bmatrix} + \begin{bmatrix} P_e^{p,0} \\ P_e^{f,0} \\ P_e^{v,0} \end{bmatrix} \tag{13}$$

where $P_e^{p,0}$, $P_e^{f,0}$, $P_e^{v,0}$ and P_e^p, P_e^f, P_e^v represent the power of the electricity load before and after participating in price-based response during peak, flat, and trough hours, respectively; $\lambda^{p,0}$, $\lambda^{f,0}$ and $\lambda^{v,0}$ represent the electricity prices during system peak, flat, and trough hours before response; $\Delta\lambda^p$, $\Delta\lambda^f$ and $\Delta\lambda^v$ represent the changes in electricity prices during peak, flat, and trough hours after response.

4. Optimization Scheduling Model

4.1. Objective Function

The optimization target for the proposed industrial park IES is to minimize the total cost, which includes procurement cost, operation and maintenance cost, wind curtailment cost, and carbon cost. The objective function is expressed in the following manner.

$$\min F = \left(C_{\text{buy}} + C_{\text{costt}} + C_{\text{W}} + C_{\text{CO}_2} \right) \tag{14}$$

where F represents the total system cost; C_{buy} represents the cost of purchased energy; C_{cost} represents the operational cost; C_W represents the cost of wind power curtailment; C_{CO_2} represents the carbon cost. The specific expressions for each component are as follows:

1. Procurement Cost

The procurement cost is composed of the costs associated with purchasing electricity, gas, and gray hydrogen for the system. It is expressed as:

$$C_{\text{buy}} = \sum_{\text{t}=1}^{T} c_{\text{t}}^{buy} P_{buy}(t) + c_{\text{g}}^{buy} \sum_{\text{t}=1}^{T} G_{buy}(t) + c_{\text{q}}^{buy} \sum_{\text{t}=1}^{T} Q_{buy}(t) \tag{15}$$

where C_{bp}, C_{bg} and C_{bq} represent the costs of purchased electricity, purchased gas, and purchased gray hydrogen, respectively; c_{t}^{bp} represents the electricity price at time t; $P_{buy}(t)$ represents the purchased electricity power at time t; c_{g}^{buy} and c_{q}^{buy} represent the unit prices of gas and gray hydrogen, respectively; $G_{buy}(t)$ and $Q_{buy}(t)$ represent the gas power and the mass of purchased gray hydrogen at time t, respectively.

2. Operation and Maintenance Cost

The operation and maintenance cost encompasses the expenses associated with the operation and maintenance of all energy-consuming and energy-storage equipment within the integrated energy system. It is expressed as:

$$C_{\text{cost}} = \sum_{\text{t}=1}^{T} [C_i P_i(t) + C_{\text{soc}} S_{\text{i}}^{d}(t) + C_{\text{soc}} S_{\text{i}}^{c}(\text{t})] \tag{16}$$

where i represents various functional devices; C_i represents the unit operational cost of energy-using devices; $P_i(t)$ represents the power usage of energy-using devices; C_{soc} represents the unit operational cost of energy storage devices; $S_{\text{i}}^{d}(t)$ and $S_{\text{i}}^{\text{c}}(t)$ represent the discharging and charging power of the energy storage device at time t, respectively.

3. Wind Curtailment Cost

$$C_{\text{w}} = c_{\text{w}} \sum_{t=1}^{T} P^{w}(t) \tag{17}$$

where c_{w} represents the penalty for wind power curtailment per unit power; $P^{w}(t)$ represents the wind power curtailment at time t.

4. Carbon Cost

The carbon cost incorporates the expenses related to carbon emissions and management within the integrated energy system. It is the sum of carbon trading costs and carbon sequestration costs and is expressed as:

$$C_{\text{CO}_2} = \sum_{\text{t}=1}^{T} C_{\text{p}}^{CO_2}(t) + C_{\text{f}}^{CO_2} \tag{18}$$

4.2. Constraints

4.2.1. Power Balance Constraint

Considering the five types of loads in the system (electricity, gas, cooling, heating, and hydrogen), maintaining a balance between supply and demand is crucial. The power balance constraint ensures that the total power supplied equals the total power consumed. This constraint is expressed as:

$$\begin{cases} P_{\text{load}}(t) = P_{\text{cchp}}(t) + P_{\text{wind}}(t) + P_1(t) + P_{\text{buy}}(t) - P_{\text{ec}}(t) - P_{\text{P2G}}(t) - P_{\text{ccs}}(t) \\ H_{\text{load}}(t) = H_{\text{gb}}(t) + H_{\text{cchp}}(t) + P_2(t) \\ C_{\text{load}}(t) = C_{\text{cchp}}(t) + C_{\text{ec}}(t) + P_3(t) \\ G_{\text{load}}(t) = G_{\text{buy}}(t) + G_{\text{MR}}(t) - G_{\text{GT}}(t) - G_{\text{gb}}(t) \\ Q_{\text{load}}(t) = Q_{\text{buy}}(t) + Q_n(t) + G_{\text{cchp}}(t) \end{cases} \tag{19}$$

where $P_{load}(t)$, $H_{load}(t)$, $C_{load}(t)$, $G_{load}(t)$ and $Q_{load}(t)$ represent the electricity, heat, gas, cooling, and hydrogen load demand at time interval t; $P_i(t)$ (i = 1, 2, 3) represents the discharging or charging power of energy storage, heating storage, and cooling storage devices at time t; $P_{H_2}(t)$ represents the mass of hydrogen storage or release at time t; $P_{cchp}(t)$, $P_{wind}(t)$ represent the power generation of the gas turbine and wind power devices at time t; $P_{ec}(t)$, $P_{P2G}(t)$ and $P_{ccs}(t)$ represent the power consumption of the electric refrigeration, electric boiler, and carbon capture system at time t; $G_{MR}(t)$ represents the gas production power of the methane reactor at time t; $G_{cchp}(t)$, $G_{gb}(t)$ represent the gas consumption power of the gas turbine and gas boiler at time t.

4.2.2. Procurement Constraints

Taking into account the system's purchasing capacity for electricity, gas, and gray hydrogen, as well as safety considerations, the procurement constraints are as follows:

$$\begin{cases} 0 \le P^{buy}(t) \le P_{buymax} \\ 0 \le G^{buy}(t) \le G_{buymax} \\ 0 \le Q^{buy}(t) \le Q_{buymax} \end{cases} \tag{20}$$

where P_{buymax}, G_{buymax}, Q_{buymax} represent the upper limits of purchased electricity, gas, and hydrogen at time t, respectively.

Equipment Ramp-up Constraint.

To ensure the safety of the equipment and the smooth operation of the system, the following limitations are imposed on the Ramp-up capability of the equipment:

$$\begin{cases} P_i^{min} \le P_i(t) \le P_i^{max} \\ \Delta P_i^d \le \Delta P_i(t) - \Delta P_i(t-1) \le \Delta P_i^u \end{cases} \tag{21}$$

where i represents different energy-consuming devices, P_i^{min} and P_i^{max} represent the lower and upper limits of device output, ΔP_i^u and ΔP_i^d represent the climbing upper and lower limits of device output, respectively.

Energy Storage Constraint.

The energy storage devices in this study encompass electricity, heat, cold, and hydrogen. Their energy charging and discharging processes are analogous. The hydrogen storage device details are provided following the Section 2.1.2, while other energy storage devices are uniformly represented as follows:

$$\begin{cases} S_i^{min} \le S_i(t) \le S_i^{max} \\ 0 \le S_i^c(t) \le S_i^{c,max} X_{cha} \\ 0 \le S_i^d(t) \le S_i^{d,max} X_{dis} \\ 0 < X_{cha} + X_{dis} < 1 \\ S_i(0) = S_i(24) \end{cases} \tag{22}$$

where $i = 1, 2, 3$ represents energy storage, heating, and cooling devices, respectively; $S_i(t)$ represents the energy storage capacity of the energy storage device at t time; $S_i^{c,max}$ and $S_i^{d,max}$ represent the maximum charging and discharging power of the energy storage device, respectively; X_{cha} and X_{dis} represents the charging and discharging state of the energy storage; $S_i(0)$ and $S_i(24)$ represent the initial and final energy storage states of the energy storage device within one scheduling cycle, respectively.

4.3. Solution Method

CPLEX, a high-performance mathematical optimization engine, integrated with MATLAB 2019b software, is widely utilized to solve complex mathematical optimization problems such as mixed-integer linear programming. In this study, given the mixed-integer

linear programming nature of the model, the CPLEX solver within MATLAB is employed to solve the proposed optimization scheduling model.

5. Case Study Analysis

The research focused on analyzing historical data from the database of a comprehensive energy system in a northern industrial park in China, including electricity, gas, cooling, heating, and hydrogen. The conventional load curves were obtained using clustering analysis. The industrial park comprises WT (Penglai Dajin Offshore Heavy Industry Co., Qingdao, China), CCHP systems (Liebherr, Qingdao, China), EC, GB, (Moon Environment Technology Co., Qingdao, China) and P2G-CCS equipment (Cockerill Jingli Hydrogen; Anhui CO_2 CAP&CONV Technology Co., LTD., Qingdao, China). The system's structure diagram is depicted in Figure 1, the primary equipment parameters are presented in Table 1, and the parameters of the energy storage devices are listed in Table 2. The analysis is performed using a 24 h scheduling cycle, taking into account seven operating scenarios to verify the efficiency and logic of the scheduling model. Moreover, the size and capacity of the equipment are uniform across all scenarios.

Table 1. Main equipment parameters.

Equipment Name	Maximum Power (kW)	Energy Conversion Efficiency	Operational Costs (CNY/kW)
GT	2000	0.44/0.39	0.0946
HRSG	500	0.9	0.032
GB	800	0.8	0.032
EC	700	5	0.0846
AC	1500	0.8	0.032
P2G	7000	EL: 0.85 MR: 0.7	0.02

Table 2. Energy storage equipment parameters.

Equipment Name	Initial Capacity	Capacity Limit	Charge/Discharge Efficiency	Operational Costs (CNY/kW)
ES	1000 kW	2000 kW	0.95	0.045
HS	800 kW	1600 kW	0.95	0.045
CS	800 kW	1600 kW	0.95	0.045
QS	20 kg	180 kg	0.95	0.045

Scenario 1: Gray hydrogen is the only hydrogen source, excluding demand response and CCS.

Scenario 2: Gray hydrogen is the hydrogen source, considering price-responsive demand, without considering CCS.

Scenario 3: Gray hydrogen is the hydrogen source, considering incentive-driven demand response, without considering CCS.

Scenario 4: Gray hydrogen is the hydrogen source, considering both price-responsive and incentive-driven demand response, without considering CCS.

Scenario 5: Gray hydrogen is the hydrogen source, considering both price-responsive and incentive-driven demand response, along with CCS.

Scenario 6: Green hydrogen produced solely through P2G is the hydrogen source, considering both price-responsive and incentive-driven demand response, along with CCS.

Scenario 7: Both gray and green hydrogen are the hydrogen sources, considering both price-responsive and incentive-driven demand response, along with CCS.

5.1. Analysis of Energy-Saving Potential for Different Demand Response Types

Figures 2 and 3 clearly demonstrate that the implementation of incentive-driven demand response results in a proactive user response to incentives between the hours of 8:00

and 21:00. Users modify their energy consumption behavior, resulting in a substantial decrease in the electricity load. By incorporating price-responsive demand, users strategically adjust their electricity usage, increasing it during the low-price period from 23:00 to early morning hours and decreasing it during peak price periods, with the goal of minimizing procurement costs. The immediate impact of price-responsive demand on reducing peak electricity consumption is more significant than that of incentive-driven demand response. The integration of both incentive-driven and price-responsive demand responses leads to a more substantial decrease in electricity load compared to utilizing each strategy separately, resulting in a more efficient load optimization.

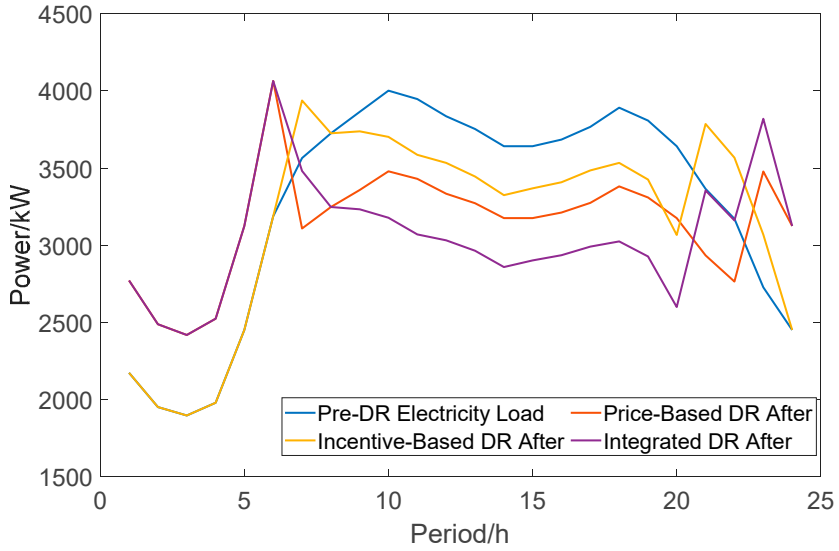

Figure 2. Comparison of electrical loads after demand response.

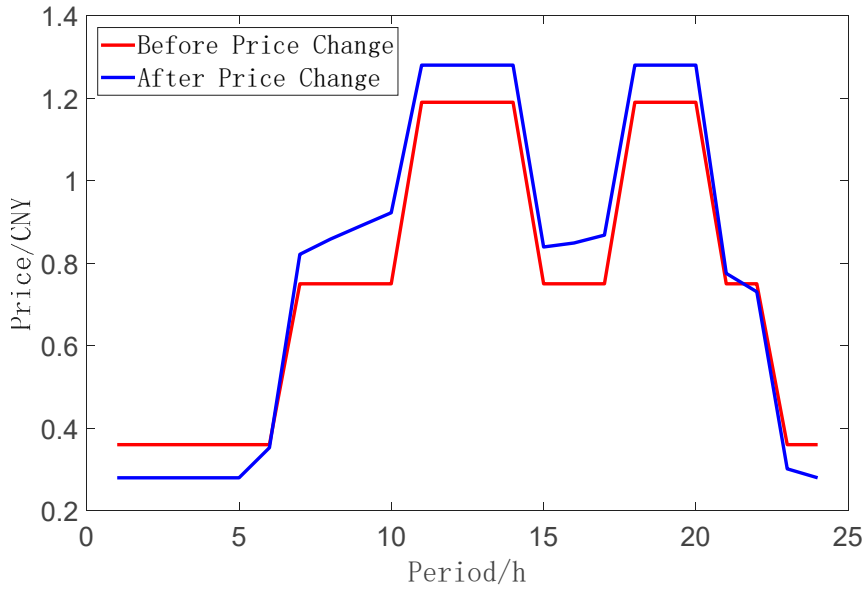

Figure 3. The electricity price variation following demand response.

Table 3 demonstrates that in Scenario 1, when demand response is not taken into account, the energy supply remains constant, leading to notably elevated total costs and carbon emissions, as well as a noticeable occurrence of wind curtailment.

Table 3. Scenarios 1–4 costs and carbon emissions.

Scenario	Total Cost (CNY)	Purchasing Energy Costs (CNY)	Wind Curtailment Cost (CNY)	Carbon Emissions (kg)
1	201,657	104,916	26,372	63,226
2	193,533	99,499	24,337	57,198
3	197,141	101,390	25,355	59,276
4	189,229	96,170	23,418	53,410

In comparison to Scenario 1, in Scenario 2, with the addition of price-responsive demand response, the system adjusts its energy supply methods flexibly to adapt to market price fluctuations, increases the proportion of wind power, leading to a reduction of 7.71% in wind curtailment costs and a decrease of 9.53% in carbon emissions. Additionally, it reallocates part of the load that was originally during peak electricity pricing periods to off-peak periods, resulting in a 5.16% reduction in purchasing energy costs and an overall cost reduction of 4.03%.

Compared to Scenario 1, in Scenario 3, with the addition of incentive-based demand response, the application of incentives effectively changes users' energy consumption habits, aligning them more closely with the grid's operational needs. This results in the shifting of some peak-period loads to nighttime when wind power generation is high, promoting the utilization of wind power and leading to a reduction of 3.86% in wind curtailment costs, a decrease of 6.25% in carbon emissions, subsequently lowering purchasing energy costs by 3.36%, and achieving an overall cost reduction of 2.24%.

Compared to Scenario 3, in Scenario 2, the electricity price signal is more effective in eliciting user responses than incentive measures. This results in a larger reduction in electricity demand, a relatively higher increase in the proportion of wind power, and significant reductions in carbon emissions and wind curtailment costs. However, the introduction of incentive measures, compared to price changes, offsets some of the reductions in total costs and purchasing energy costs. As a result, the reduction in purchasing energy costs and overall costs in Scenario 3 is not as significant as in Scenario 2.

Scenario 4, which simultaneously considers both price-responsive and incentive-based demand response, operates with the combined effects of price mechanisms and incentive measures. During peak load periods, the electricity price increases due to the simultaneous action of pricing mechanisms and incentives. As a result, some users shift their high-demand periods to the low-price periods when wind power is abundant, further increasing the proportion of wind power. This leads to an 11.20% reduction in wind curtailment costs. Moreover, during peak load periods, CCHP and wind power generation can meet more demand, reducing the proportion of purchased energy and corresponding costs by 8.34%. The associated carbon emissions from purchased energy decrease, resulting in a 15.60% reduction in the overall system carbon emissions. Carbon trading costs also decrease, contributing to a 6.16% reduction in the overall system costs. Therefore, simultaneously considering both types of demand response can further promote peak shaving, accommodate new energy sources, and significantly reduce carbon emissions.

5.2. Impact Analysis of CCS on Economic Viability

Figure 4 illustrates the introduction of CCS in Scenario 5. CCS has high energy consumption properties; therefore, when wind power generation is minimal, the electricity produced by CCHP combined with the initially acquired electricity is not enough to meet the power requirement of the system. As a result, there is a need to buy more electricity, which leads to a 2.99% rise in the expenses of acquiring energy compared to Scenario 4.

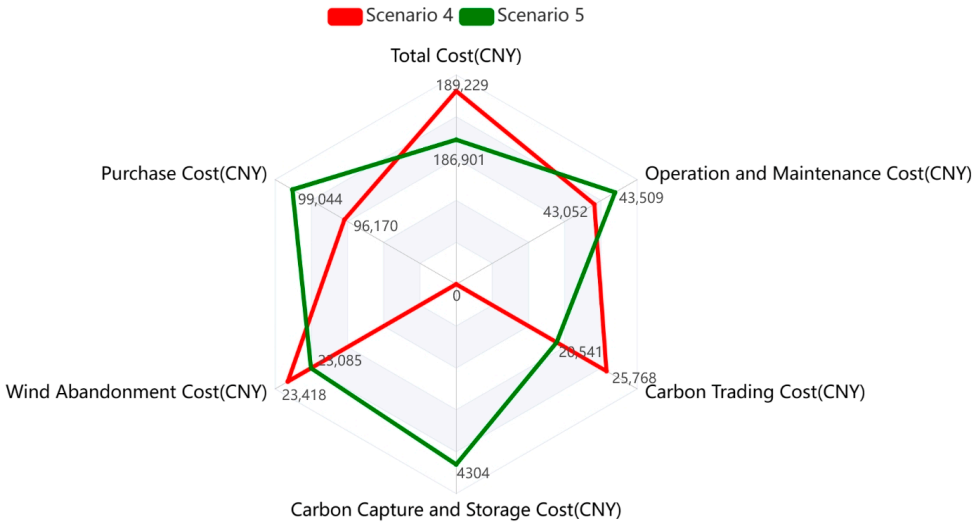

Figure 4. Scenario 4 and Scenario 5 cost comparison.

During the operation of CCS, the system must efficiently utilize the captured CO_2 by using a portion of it for the synthesis of hydrogen and methane, which will serve as a carbon source. Additional allocation is required to isolate another section, hence augmenting the expenses linked to carbon capture and storage. Additionally, the expenses associated with maintaining the CCS operation are taken into account, resulting in a proportional rise of 1.06% in operational costs. However, the considerable uptake of CO_2 by CCS during operation effectively decreases the carbon emissions of the system, resulting in a 20.28% decrease in carbon trading expenses and a notable improvement in economic feasibility.

Furthermore, when wind power generation is strong, CCS prioritizes using wind power to meet its energy requirements, leading to a decrease of 1.42% in wind curtailment costs and an overall cost reduction of 1.23%. Although the implementation of CCS incurs extra expenses, its remarkable capacity to reduce carbon emissions and integrate renewable energy significantly impacts the economic feasibility of the system.

5.3. Carbon Reduction Benefits Analysis of Green Hydrogen

Figure 5 illustrates that in Scenario 5, the implementation of CCS results in a substantial reduction of the system's carbon emissions. Specifically, there is a noteworthy decrease of 56.09% compared to Scenario 4. Furthermore, as a result of the implementation of tiered carbon emissions, there is a marginal decrease in overall expenses. Nevertheless, as the carbon emissions linked to gray hydrogen are solely accounted for in carbon quota trading and do not really contribute to emissions inside the system, the carbon emissions from gray hydrogen remain unaltered.

Scenario 6 only relies on P2G technology for green hydrogen production, resulting in very poor efficiency. This process demands a significant electrical supply. Due to the inadequacy of wind power generation alone, it is necessary to enhance CCHP electricity output and substantially boost electricity purchasing. This leads to a 12.6-fold increase in carbon emissions compared to Scenario 5 and a corresponding 21.33% increase in total expenses.

In Scenario 7, prioritizing the use of wind power for green hydrogen production and supplementing with gray hydrogen as needed, the system efficiently accommodates wind power, reducing wind curtailment costs and dramatically cutting the use of gray hydrogen. The system's carbon emissions are reduced by 40.98% and 93.30% in comparison to the use of gray hydrogen and green hydrogen individually. Consequently, total costs reduce by 17.93% and 32.35%. This highlights the capacity of the integrated energy system to strategically manage the cost differentials between gray hydrogen (which is cheaper but has higher carbon emissions) and green hydrogen (which is more expensive but has lower carbon emissions) in response to fluctuating carbon prices. By flexibly adjusting the proportion of gray hydrogen and green hydrogen, the system maximizes its economic benefits.

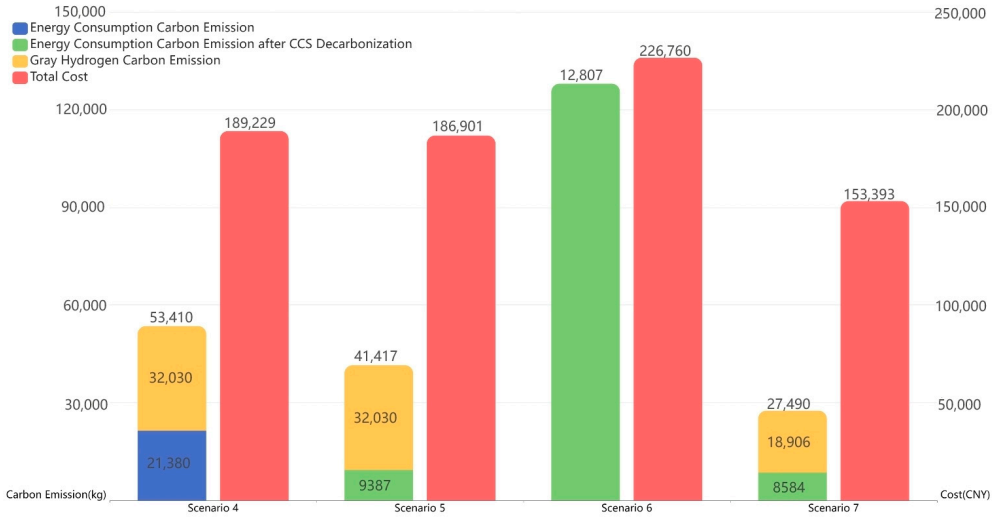

Figure 5. Scenario 4–7 carbon emissions and cost comparison.

5.4. Equipment Operation Analysis

Figure 6 shows that throughout the time periods 1 to 7 and 20 to 24, a significant amount of wind power is being created. Most of this electricity is being used to create green hydrogen through P2G devices. Within this time period, green hydrogen is utilized to fulfill the need for hydrogen, and it also undergoes methanation in the methane reactor to meet a portion of the gas load requirements. A further fraction of the hydrogen is held in dedicated hydrogen tanks, primarily intended for giving hydrogen to consumers between 6 a.m. and 8 a.m. Some of the electricity produced is used to power the carbon capture system and meet certain electricity demands.

The CCHP system consistently functions at a high level, maximizing its outstanding economic advantages. The process involves the utilization of natural gas to generate electricity as well as to offer cooling and heating. Additionally, it has the capability to store any surplus energy. Between 10 a.m. and 6 p.m., the decrease in wind power production results in an inadequate supply of electricity from the combination of wind power and gas turbine generation to fulfill the demand. The grid is connected to an external power supply, and in order to reduce the expenses of acquiring energy, energy storage devices start discharging to relieve the strain on the electrical supply.

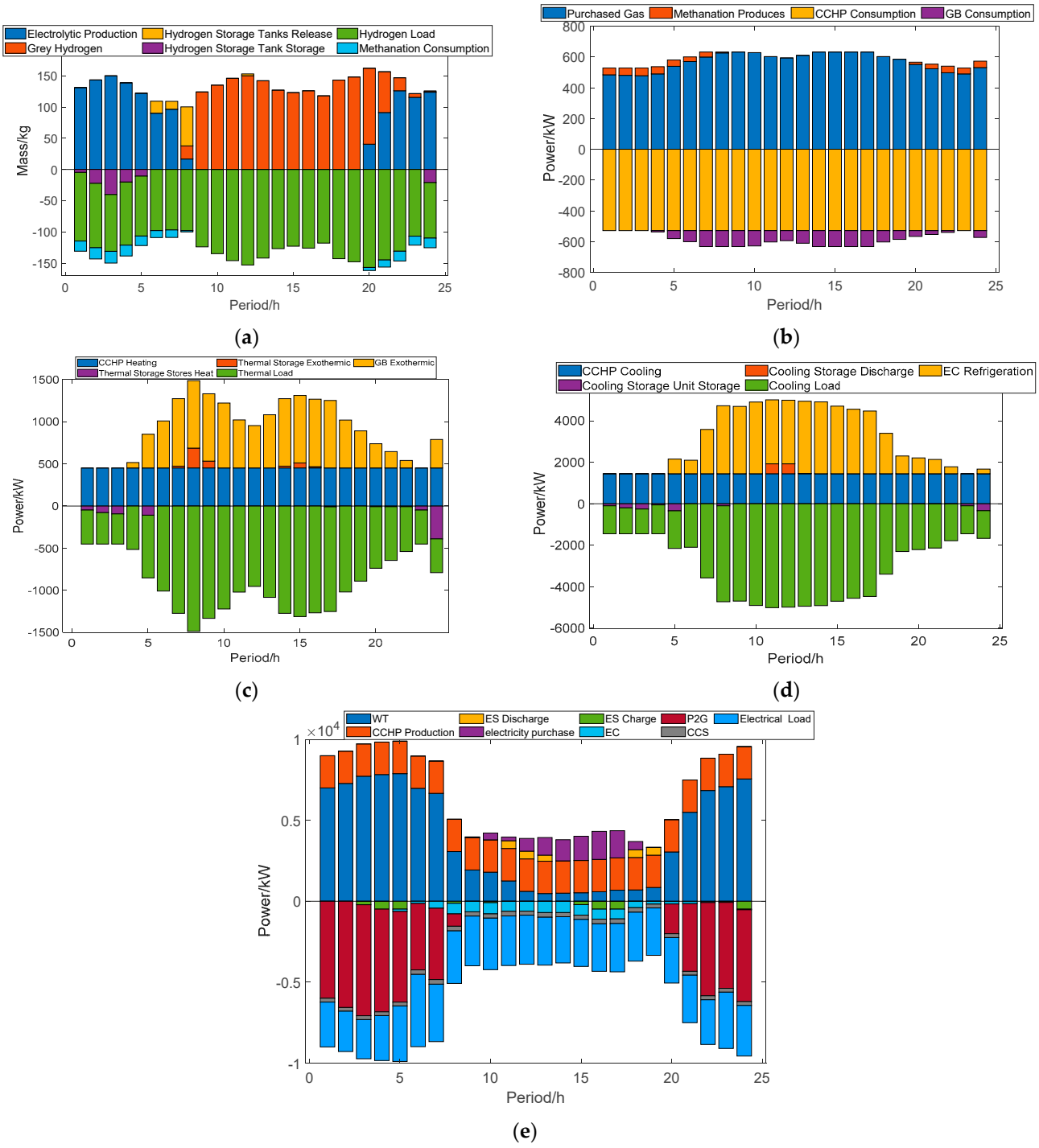

Figure 6. Scenario 7 load balancing chart (**a**) Hydrogen Load Balance Chart; (**b**) Gas Load Balance Chart; (**c**) Heating Load Balance Chart; (**d**) Cooling Load Balance Chart; (**e**) Electric Load Balance Chart.

6. Discussion

The low-carbon economic scheduling technique described in this work for the industrial park IES takes into account the carbon reduction benefits of replacing some carbon-intensive gray hydrogen with green hydrogen produced by P2G, in contrast to typical scheduling methods. Existing research on P2G predominantly focuses on P2G as a complete entity in terms of system carbon emissions and the integration of renewable energy. However, there has been a notable oversight in analyzing the carbon reduction potential of

green hydrogen produced through the P2G process as a hydrogen source. Therefore, this paper addresses this gap in research by conducting an in-depth analysis in this specific area. By strategically allocating green and gray hydrogen within a coordinated supply, the system can leverage the environmental advantages associated with green hydrogen while maintaining the cost benefits typically associated with gray hydrogen. This achieves an effective balance between economic feasibility and environmental sustainability.

Furthermore, the integration of P2G with CCS creates a closed-loop system that captures CO_2 emissions and recycles them back into hydrogen and methane production. This closed-loop reuse of carbon enabled by P2G-CCS coupling improves the carbon efficiency of the overall system. The exceptional carbon capture capability of CCS paired with the green hydrogen production of P2G allows the system to achieve substantial reductions in carbon emissions, hence improving total economic advantages.

Currently, the majority of research on demand response primarily focuses on the impact of individual demand response mechanisms on system economics and energy efficiency. Limited attention has been given to exploring the variations in energy-saving effects among different demand response strategies and the combined influence of employing two distinct demand response approaches simultaneously. Thus, this paper delves into an investigation in this area to fill this research gap. The effectiveness of price-based demand response depends on the real-time electricity pricing and the sensitivity of users to price fluctuations. On the other hand, the effectiveness of incentive-based demand response is linked to the design of incentive measures and the willingness of users to respond. When utilized independently, both methods can only encourage users to alter their electricity consumption habits within a limited range. Their peak-shifting capabilities are consequently constrained. In the short term, price-based demand response tends to yield more favorable outcomes compared to incentive-based demand response. However, their combined application allows for better optimization of the load curve, reducing peak-to-valley differentials and promoting coordinated development of economic and environmental benefits in the system.

Nevertheless, there were certain limitations in this investigation that could be addressed in future work. The demand response parameters used in the model were relatively simple and did not fully capture the stochastic nature of user reactions. More complex demand response models could be developed to better represent the probabilistic behaviors of users. The economic model was also somewhat simplified, and in practice, transaction prices can be influenced by many other factors besides just supply and demand. A more comprehensive economic model could be constructed to account for additional market dynamics like competition between suppliers, bargaining power, information asymmetry, and so on.

Subsequent investigations can prioritize the following facets:

(i) Developing a framework for the auctioning system in the carbon trading market. Create a competitive bidding model for the carbon trading market that aims to maximize carbon trading pricing by taking into account market dynamics and participant strategies.
(ii) Integrating electricity market transactions. Examine electricity market transactions and develop a competitive bidding model for multi-energy coupling, improving the integration of different energy sources and optimizing market interactions.
(iii) Improving the simulation of user responses. Enhance the modeling of user responses by considering the probabilistic nature of user behavior in order to enhance the precision of demand response forecasts.

This work offers a novel viewpoint on low-carbon scheduling in IES within the context of tiered carbon trading. However, it acknowledges specific limits that necessitate additional refinement and development. In order to achieve coordinated and sustainable development in terms of economic, environmental, and sociological variables, future research should focus on creating a more comprehensive and accurate representation of demand response and economic models. Continual improvements in models and

approaches are anticipated to enhance the importance of low-carbon scheduling strategies, hence aiding the attainment of dual-carbon objectives.

7. Conclusions

This research presents a hydrogen-IES low-carbon economic dispatch method under tiered carbon pricing, using two demand response scenarios, in order to address the hydrogen demand of an industrial park. The research purpose of using P2G to produce green hydrogen to replace part of gray hydrogen as a hydrogen source to balance carbon emission reduction and economy and to absorb a large amount of renewable energy has been realized. Based on the examination of the cases, the following conclusions are derived:

By employing P2G technology to produce green hydrogen, it becomes possible to substitute a portion of gray hydrogen as the hydrogen source. This approach enables the full exploitation of the advantages of high green hydrogen pricing and low-carbon emissions while also making use of low gray hydrogen costs and large carbon emissions. This leads to a substantial drop in carbon emissions from the system, resulting in lower carbon costs and wind curtailment costs. As a result, the overall economic efficiency of the system is improved.

Various forms of demand response contribute to the reduction of peak electricity consumption and the optimization of load management. Price-based demand response has a direct effect on power prices, and in the short term, it is more readily accepted by users compared to incentive-based responses. The impact of price-based demand response on the load is more significant, resulting in a higher potential for energy savings.

Integrating CCS into the IES leads to higher purchase energy costs and operational costs as a result of its high energy consumption characteristics. Nevertheless, the remarkable carbon reduction impact of CCS substantially decreases the expenses associated with carbon trading, resulting in a further decrease in overall costs.

Author Contributions: Writing—original draft preparation, B.S.; methodology, R.W.; supervision, M.W. (Ming Wang); software, M.W. (Mingyuan Wang); conceptualization, Q.Z.; writing—review and editing, Y.L.; resources, H.G. All authors have read and agreed to the published version of the manuscript.

Funding: This research was funded by the National Natural Science Foundation of China (no. 62073196, 62133008); the Natural Science Foundation of Shandong Province (no. ZR2019ZD09); and the Key Research and Development Project of Shandong Province (2019JZZY010903). This research was supported by the Taishan Industrial Experts Program (no. tscx202312127) and the State Grid Science and Technology Project (5100-202116567A-0-5-SF).

Institutional Review Board Statement: Not applicable.

Informed Consent Statement: Not applicable.

Data Availability Statement: The raw data supporting the conclusions of this article will be made available by the authors on request.

Conflicts of Interest: Author Ruiqi Wang was employed by the company State Grid Shandong Integrated Energy Services Co., Ltd. and author He Gao was employed by the company Shandong Zhengchen Technology Co., Ltd. The remaining authors declare that the re-search was conducted in the absence of any commercial or financial relationships that could be construed as a potential conflict of interest.

References

1. Zeng, N.; Jiang, K.; Han, P.; Hausfather, Z.; Cao, J.; Kirk-Davidoff, D.; Ali, S.; Zhou, S. The Chinese carbon-neutral goal: Challenges and prospects. *Adv. Atmos. Sci.* **2022**, *39*, 1229–1238. [CrossRef] [PubMed]
2. Pan, C.; Jin, T.; Li, N.; Wang, G.; Hou, X.; Gu, Y. Multi-objective and two-stage optimization study of integrated energy systems considering P2G and integrated demand responses. *Energy* **2023**, *270*, 126846. [CrossRef]
3. Li, Y.; Han, M.; Shahidehpour, M.; Li, J.; Long, C. Data-driven distributionally robust scheduling of community integrated energy systems with uncertain renewable generations considering integrated demand response. *Appl. Energy* **2023**, *335*, 120749. [CrossRef]

4. Lepage, T.; Kammoun, M.; Schmetz, Q.; Richel, A. Biomass-to-hydrogen: A review of main routes production, processes evaluation and techno-economical assessment. *Biomass Bioenergy* **2021**, *144*, 105920. [CrossRef]
5. Li, G.; Cui, P.; Wang, Y.; Liu, Z.; Zhu, Z.; Yang, S. Life cycle energy consumption and GHG emissions of biomass-to-hydrogen process in comparison with coal-to-hydrogen process. *Energy* **2020**, *191*, 116588. [CrossRef]
6. Alabbadi, A.A.; Obaid, O.A.; AlZahrani, A.A. A comparative economic study of nuclear hydrogen production, storage, and transportation. *Int. J. Hydrogen Energy* **2024**, *54*, 849–863. [CrossRef]
7. El-Emam, R.S.; Ozcan, H.; Zamfirescu, C. Updates on promising thermochemical cycles for clean hydrogen production using nuclear energy. *J. Clean. Prod.* **2020**, *262*, 121424. [CrossRef]
8. Liu, J.; Sun, W.; Harrison, G.P. Optimal low-carbon economic environmental dispatch of hybrid electricity-natural gas energy systems considering P2G. *Energies* **2019**, *12*, 1355. [CrossRef]
9. Yang, J.; Zhang, N.; Cheng, Y.; Kang, C.; Xia, Q. Modeling the operation mechanism of combined P2G and gas-fired plant with CO_2 recycling. *IEEE Trans. Smart Grid* **2018**, *10*, 1111–1121. [CrossRef]
10. De Corato, A.; Saedi, I.; Riaz, S.; Mancarella, P. Aggregated flexibility from multiple power-to-gas units in integrated electricity-gas-hydrogen distribution systems. *Electr. Power Syst. Res.* **2022**, *212*, 108409. [CrossRef]
11. Son, Y.G.; Choi, S.; Aquah, M.A.; Kim, S.Y. Systematic planning of power-to-gas for improving photovoltaic acceptance rate: Application of the potential RES penetration index. *Appl. Energy* **2023**, *349*, 121611. [CrossRef]
12. Abdin, Z.; Colin, J.W.; Gray, E. Modeling and simulation of a proton exchange membrane (PEM) electrolyser cell. *Int. J. Hydrogen Energy* **2015**, *40*, 13243–13257. [CrossRef]
13. Marangio, F.; Santarelli, M.G.L.; Michele, C. Theoretical model and experimental analysis of a high pressure PEM water electrolyser for hydrogen production. *Int. J. Hydrogen Energy* **2009**, *34*, 11431158. [CrossRef]
14. Luo, Z.; Wang, J.; Xiao, N.; Yang, L.; Zhao, W.; Geng, J.; Lu, T.; Luo, M.; Dong, C. Low Carbon Economic Dispatch Optimization of Regional Integrated Energy Systems Considering Heating Network and P2G. *Energies* **2022**, *15*, 5494. [CrossRef]
15. Mansouri, S.A.; Ahmarinejad, A.; Nematbakhsh, E.; Javadi, M.S.; Jordehi, A.R.; Catalão, J.P.S. Energy hub design in the presence of P2G system considering the variable efficiencies of gas-fired converters. In Proceedings of the 2021 International Conference on Smart Energy Systems and Technologies (SEST), Vaasa, Finland, 6–8 September 2021; pp. 1–6.
16. Zhang, Z.; Du, J.; Zhu, K.; Guo, J.; Li, M.; Xu, T. Retracted: Optimization scheduling of virtual power plant with carbon capture and waste incineration considering P2G coordination. *Energy Rep.* **2022**, *8*, 7200–7218. [CrossRef]
17. Alizad, E.; Rastegar, H.; Hasanzad, F. Dynamic planning of Power-to-Gas integrated energy hub considering demand response programs and future market conditions. *Int. J. Electr. Power Energy Syst.* **2022**, *143*, 108503. [CrossRef]
18. Zhang, Z.; Du, J.; Li, M.; Guo, J.; Xu, Z.; Li, W. Bi-level optimization dispatch of integrated-energy systems with P2G and carbon capture. *Front. Energy Res.* **2022**, *9*, 784703. [CrossRef]
19. Majidi, M.; Nojavan, S.; Zare, K. Optimal stochastic short-term thermal and electrical operation of fuel cell/photovoltaic/battery/grid hybrid energy system in the presence of demand response program. *Energy Convers. Manag.* **2017**, *144*, 132–142. [CrossRef]
20. Zhang, Y.; Liu, Z.; Wu, Y.; Li, L. Research on Optimal Operation of Regional Integrated Energy Systems in View of Demand Response and Improved Carbon Trading. *Appl. Sci.* **2023**, *13*, 6561. [CrossRef]
21. Fleschutz, M.; Bohlayer, M.; Braun, M.; Henze, G.; Murphy, M.D. The effect of price-based demand response on carbon emissions in European electricity markets: The importance of adequate carbon prices. *Appl. Energy* **2021**, *295*, 117040. [CrossRef]
22. Pandey, V.C.; Gupta, N.; Niazi, K.R.; Swarnkar, A. An economic price based demand response using overlapping generation model in distribution systems. *Electr. Power Syst. Res.* **2022**, *213*, 108794. [CrossRef]
23. Amin, M.M.; Yazdankhah, A.S.; Mohammadi-Ivatloo, B. Stochastic security-constrained operation of wind and hydrogen energy storage systems integrated with price-based demand response. *Int. J. Hydrogen Energy* **2019**, *44*, 14217–14227.
24. Tavakkoli, M.; Fattaheian-Dehkordi, S.; Pourakbari-Kasmaei, M.; Liski, M.; Lehtonen, M. Bonus-based demand response using Stackelberg game approach for residential end-users equipped with HVAC system. *IEEE Trans. Sustain. Energy* **2020**, *12*, 234–249. [CrossRef]
25. Van Tilburg, J.; Siebert, L.C.; Cremer, J.L. MARL-iDR: Multi-Agent Reinforcement Learning for Incentive-based Residential Demand Response. *arXiv* **2023**, arXiv:2304.04086.
26. Raman, G.; Zhao, B.; Peng, J.C.-H.; Weidlich, M. Adaptive incentive-based demand response with distributed non-compliance assessment. *Appl. Energy* **2022**, *326*, 119998. [CrossRef]
27. Shi, Q.; Chen, C.-F.; Mammoli, A.; Li, F. Estimating the profile of incentive-based demand response (IBDR) by integrating technical models and social-behavioral factors. *IEEE Trans. Smart Grid* **2019**, *11*, 171–183. [CrossRef]
28. Chen, Z.; Zhang, Y.; Tang, W.; Lin, X.; Li, Q. Generic modelling and optimal day-ahead dispatch of micro-energy system considering the price-based integrated demand response. *Energy* **2019**, *176*, 171–183. [CrossRef]